Universiteit
Leiden
The Netherlands

Computational optimisation of optical projection tomography for 3D image analysis

Tang, X.

Citation
Tang, X. (2020, June 10). *Computational optimisation of optical projection tomography for 3D image analysis*. Retrieved from https://hdl.handle.net/1887/106088

Version:	Publisher's Version
License:	Licence agreement concerning inclusion of doctoral thesis in the Institutional Repository of the University of Leiden
Downloaded from:	https://hdl.handle.net/1887/106088

Note: To cite this publication please use the final published version (if applicable).

Cover Page

Universiteit Leiden

The handle http://hdl.handle.net/1887/106088 holds various files of this Leiden University dissertation.

Author: Tang, X.
Title: Computational optimisation of optical projection tomography for 3D image analysis
Issue Date: 2020-06-10

Chapter 4

Segmentation-driven Optimisation for Iterative Reconstruction in Optical Projection Tomography: An Exploration

This chapter is based on the following publication:

Tang X and Verbeek F.J. Segmentation-driven Optimisation for Iterative Reconstruction in Optical Projection Tomography: An Exploration. *IEEE Transactions on Computational Imaging*. (under review)

Chapter summary

The reconstruction of a tomogram to a 3D image has some drawbacks in that there are artefacts introduced in the reconstruction that affect the quality of the image. We have been using the filtered back projection algorithm for the reconstruction; but iterative reconstruction algorithms demonstrate a superior performance as far as artefacts are concerned. In computerized tomography these iterative algorithms are successfully applied. These iterative algorithms will, however, require much more computation time.

In this chapter we study capability of iterative algorithms to remove streak artefacts from reconstructions of optical projection tomograms. Moreover, we explore possible ways to optimize the most customary parameters of the iterative reconstruction algorithms so as to improve its reconstruction performance. Due to the lack of benchmarks for direct reconstruction evaluation in optical projection tomography we consider the assessment according to the performance of segmentation in the reconstruction. We use the zebrafish model, the model system for which our OPT system is used a lot, as we can easily obtain data and build a benchmark. For the segmentation approach we employed the 2D U-net convolutional neural network as it is known for good performance in biomedical image segmentation.

4.1 Introduction

Three dimensional (3D) image reconstruction in OPT can play a crucial role in giving insight into protein distribution and/or gene expression within a research model, e.g. zebrafish, at a tissue and organ level. Given the specific data, a good reconstruction algorithm typically produces a reliable and effective 3D reconstruction, whereas a simple reconstruction technique may introduce computational artefacts that hamper the interpretation of the data. These kinds of artefacts are introduced during the reconstruction process because of imperfection of the data prior to the imaging process. There are two categories of approaches to reduce or eliminate these artefacts. One is considering the perspective of the imaging process, meaning trying to avoid the imaging imperfections that results in artefacts, either from the sample side or from the instrument side. This approach is, however, sometimes quite expensive or even unachievable in some cases. Another category is to computationally improve the reconstruction from an imperfect tomogram. It can be either applying a powerful reconstruction algorithm or employing pre-processing and/or post-processing of a specific algorithm.

In 2005, Walls *et al.* [22] first presented the possible artefacts in the Filtered Back Projection (FBP) reconstruction existing in an OPT imaging system. The main contribution of this work lies in the study of the origins of the reconstruction artefacts from the imaging source, for instance signal decay, CCD imperfection, etc. He studied the reasons why these imperfections in imaging would result in reconstruction artefacts within the FBP [68] framework, but not yet explain if more advanced reconstruction algorithms, such as iterative reconstruction, can reduce or even eliminate these artefacts.

In addition to the work of Walls *et al*., we explain the so called streak artefacts in the FBP reconstruction and briefly explain the imaging source reason. OPT imaging is characterized by its wide depth of field (DoF) compared to high-resolution microscopes, e.g. confocal microscopy [69], [70]. This means that a point source that is properly focused in one angle of rotation may be blurred or even invisible in its opposite angle. This will result in streak artefacts in the FBP reconstruction because of the severe asymmetry of tomograms.

In CT imaging, the so called metal artefacts can be either reduced with artefacts reduction algorithm within the FBP framework or eliminated by using other reconstruction methods such as iterative reconstruction. With respect to reduction of artefacts, in the last two decades a variety of approaches have been proposed for CT [71]–[75]. These approaches, however, can only decrease the artefacts rather than eliminate them. As for streak artefacts, elimination using other reconstruction methods, the iterative reconstruction stands out. Inspired by the superior performance of metal artefacts elimination when using iterative reconstruction in CT [35], [76]–[78], we are interested in exploring its capability of streak artefacts elimination in OPT.

Iterative reconstruction refers to iterative algorithmic approaches used to reconstruct 2D or 3D images from tomographic imaging techniques. Generally, it starts with an

assumed image, computes projections from the image via a projection function and updates the image according to the difference between the calculated and the actual projections. According to the updating schema for image, it can be categorized into four kinds of approaches, i.e. algebraic reconstruction techniques (ART) [23], iterative sparse asymptotic minimum variance (SAMV) [24], statistical reconstruction [25] and learned iterative reconstruction [26], [79]. They are considered superior when there is a lack of uniform projections or when the projections are sparse, which to some extent fits the character of imaging source for the aforementioned streak artefacts in OPT. Compared to its application in CT, iterative reconstruction was less studied in OPT. Correia *et. al* [12] applied the iterative reconstruction to achieve relatively reasonable results on a sparse collection of projections in 2015. One possible reason for impeding prevalence of iterative reconstruction in OPT is the high computation time. Nevertheless, with the rapid development of computational strategies, e.g. parallel computing and GPU, iterative reconstruction will be more widely used in OPT.

The common approach for evaluating reconstruction performance in tomographic imaging is accomplished by producing and projecting a simulated object, e.g. phantom in CT, and assessing the performance of a reconstruction algorithm based on the projections [80]. Nevertheless, due to the DoF in OPT imaging the projection function is much more complicated than that in CT. In this case, simulating the projections of a phantom as benchmark has, to our best knowledge, never happened in OPT. Therefore, as an alternative we use images from real-life samples for experiments.

Iterative reconstruction has great potential for image reconstruction in OPT. However, there is an intrinsic disadvantage for image reconstruction in OPT in that a good quantitative evaluation on the reconstruction is difficult. This disadvantage mainly results from the lack of benchmarks for samples. In such a situation formulating an alternative evaluation method according to the specific research problem is considered applicable and feasible. With this idea we transfer the evaluation of reconstruction to that of segmentation which can be easily obtained given the reconstruction data; in our experiments we use zebrafish. The inspiration of the transfer originates from the fact that we are expecting better segmentation results from different reconstructions on the same data. Therefore, this transfer can be valid under the assumption that the reconstruction with better segmentation result is preferred, given effect of the same segmentation algorithm. By transferring the evaluation of reconstruction to segmentation, we can approximate the best parameters for reconstruction. Thus, our approach can be interpreted as an optimisation of iterative reconstruction for OPT.

In this chapter we focus on iterative reconstruction in OPT so as to avoid streak artefacts, and furthermore we explore the possibility of segmentation evaluation to optimize the parameters for iterative reconstruction. In section 4.2 the implementation of iterative reconstruction will be briefly introduced. We will focus on the parameter optimisation in section 4.3. The specific scheme and approach for parameter optimisation will be exhaustively discussed there, which will be followed by the experimental results

and discussion. Finally we present our conclusions, as well as raise some limitations and future work.

4.2 Iterative reconstruction for OPT

In general, iterative reconstruction can lead to a more accurate OPT 3D image than that obtained by the FBP [68]. However, a large number of iterations may be required to generate an acceptable result, with each iteration taking about the same amount of time as the FBP. Thus to some extent the effectiveness of iterative reconstruction is achieved at the expense of more computation time. One approach to reduce the number of iterations is to organize the projection data into a series of ordered subsets of evenly spaced projections and update the current estimate of the object after each subset rather than after the complete set of projections. The most commonly used algorithm employing subset is referred to as ordered subset expectation maximization (OSEM) reconstruction [28], [81]. It improves the efficiency of iterative reconstruction with respect to computational time.

According to the expectation maximization (EM) algorithm in iterative reconstruction [82], the intensity of an object projected to the detector follows the Poisson distribution with expected value $\mu = E(I_{(z,\beta,\theta)}) = P_{(z,\beta,\theta)} \times R_{(x,y,z)}$). The object to be reconstructed is assumed as $R_{(x,y,z)}$ and will be updated in an iterative way as follows:

$$R^{l+1}_{(x,y,z)} = R^{l}_{(x,y,z)} \frac{\sum_{\theta_t \in I_t} (I_{(z,\beta,\theta_t)} / (P_{(z,\beta,\theta_t)} \times R^{l}_{(x,y,z)}))}{\sum_{\theta_t \in I_t} P_{(z,\beta,\theta_t)}} \quad (1)$$

with P being the projection function while $I_{(z,\beta,\theta)}$ symbolizes the tomogram at the angle θ in OPT. (z, β, θ) and $(x, y, z)$are separately the tomogram and 3D image coordinate, with β being the detector axis and θ being the projection angle; whilst z is the slice number and (x, y) indicates the image size of a reconstructed slice. The EM based iterative reconstruction is based on the idea that the reconstruction $R_{(x,y,z)}$ of an object in 3D space can be estimated with the observed or measured data $I_{(z,\beta,\theta)}$ by iteratively updating $R_{(x,y,z)}$ with the EM algorithm, with l being the iteration step. The conventional EM iterative reconstruction updates $R_{(x,y,z)}$ based on a full set of observation I, while the OSEM splits the full set into T ordered subsets $I = \{I_t : t = 1,2, \dots, T\}$, $I_t = I_{(z,\beta,\theta_t)}$ and implements the updating based on I_t in each iteration step [82].

In the OPT imaging system, the light is approximately considered as parallel rather than conical. In this case the projection function $P_{(z,\beta,\theta_t)}$ remains the same at different z positions or on different reconstructed slices. Then the update can be implemented on a slice by slice basis, with each slice updated using:

$$R^{l+1}_{(x,y)} = R^{l}_{(x,y)} \frac{\sum_{\theta_t \in I_t} (I_{(\beta,\theta_t)} / (P_{(\beta,\theta_t)} \times R^{l}_{(x,y)}))}{\sum_{\theta_t \in I_t} P_{(\beta,\theta_t)}} \quad (2)$$

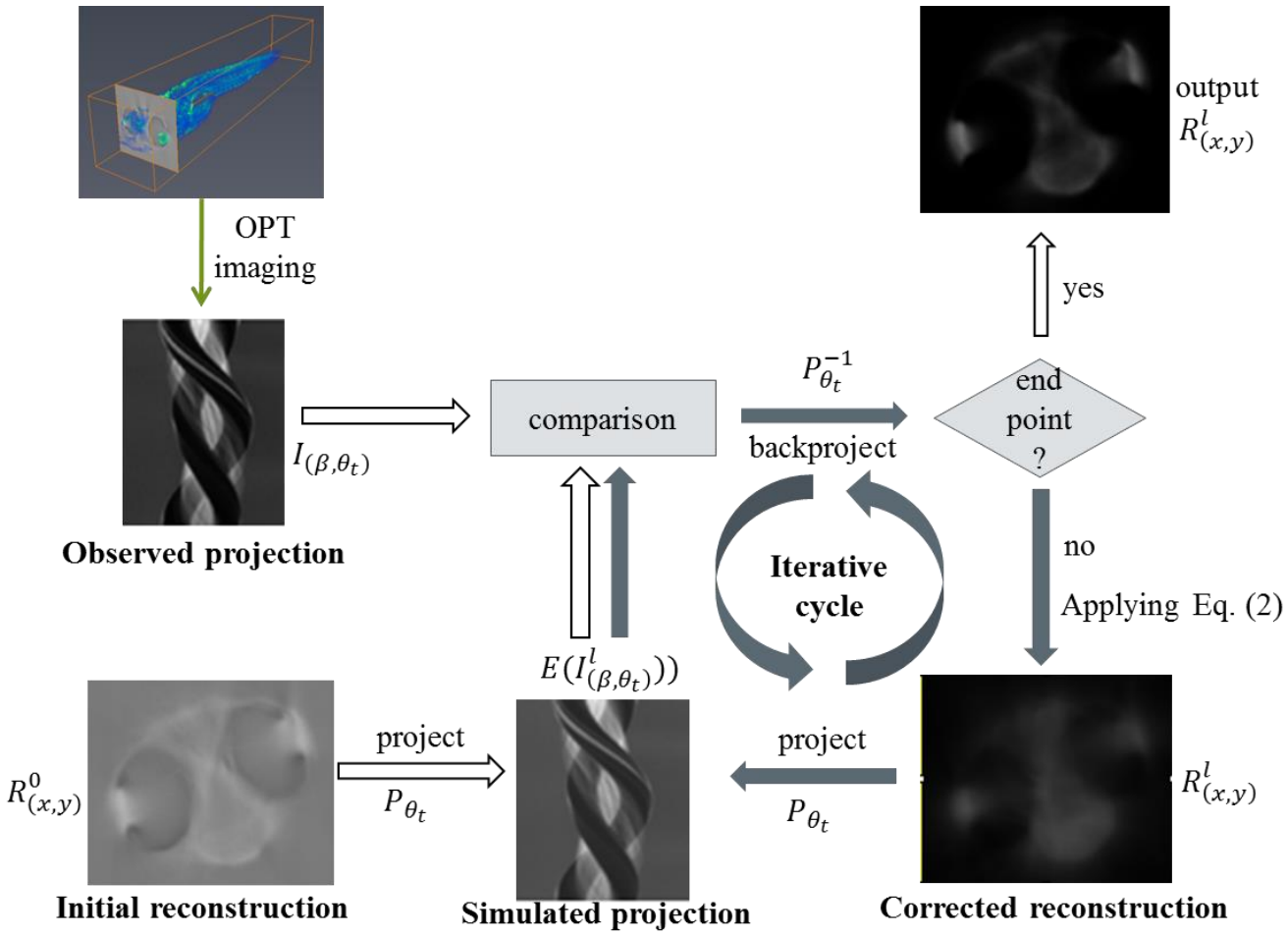

Figure 4.1. Workflow of iterative reconstruction in OPT. Example is given on a zebrafish larvae of 6 days post fertilization (*dpf*).

In Figure 4.1 the workflow of iterative reconstruction is depicted as applied on a zebrafish sample on a slice-by-slice basis. The observed projections, are acquired from the OPT imaging system and are here defined as the sinogram $I_{(\beta,\theta_t)}$. By using the OSEM algorithm, the reconstructed slice $R^l_{(x,y)}$ is updated based on the differences between the observed projection and the simulated projection in reconstruction space using Eq. (2), with a initial reconstruction slice $R^0_{(x,y)}$. The simulated projection is updated as $E(I^l_{(\beta,\theta_t)}) = (P_{\theta_t} \times R^l_{(x,y)})$and $E(I^0_{(\beta,\theta_t)}) = (P_{\theta_t} \times R^0_{(x,y)})$ for the first update. This difference $I_{(\beta,\theta_t)}/E(I^l_{(\beta,\theta_t)})$ in projection space is reconstructed to 3D image space using back projection $P^{-1}_{\theta_t}$, which is finally used for updating the slice $R^l_{(x,y)}$ as shown in Eq. (2). As we can see from Figure 4.1, in the iterative framework both the end point and the initial reconstruction $R^0_{(x,y)}$ play an important role in the final results, which will be studied in the following sections.

4.3 Parameter optimisation for iterative reconstruction

Parameters for iterative reconstruction can be optimized based on the performance assessed on reconstructed results. Nevertheless, due to the lack of benchmark for direct reconstruction evaluation in optical projection tomography we consider the assessment according to the segmentation performance of the 3D images reconstructed with different parameters. To this end, the framework for this idea will be first elaborated. It is proposed under the assumption that the segmentation method used is reliable and effective. In order to guarantee this, we employ a convolutional neural network (CNN) as it is known for its high performance in image segmentation. In Figure 4.2, an example slice (head part) of 25 *dpf* zebrafish is given, explaining how different reconstruction parameters influence the segmentation performance. Figure 4.2 (a) and (b) are two slices reconstructed from the iterative reconstruction using different parameters. Figure 4.2 (c) and (d) show the corresponding segmentation results based on the reconstructed slices from Figure 4.2 (a) and (b). The benchmark of this slice is displayed in (e), which is obtained from the manual segmentation. When visually comparing the reconstructed slices and the segmentation performance, we observe that different reconstruction parameters could produce different 3D image slices, which will consequently result in distinct segmentation results. For instance the slice in (b) has better segmentation performance shown in (d), comparing to the performance (c) from the slice in (a). With this assumption, we can optimize the parameters based on the segmentation performance of the 3D image slices that are reconstructed with different parameters.

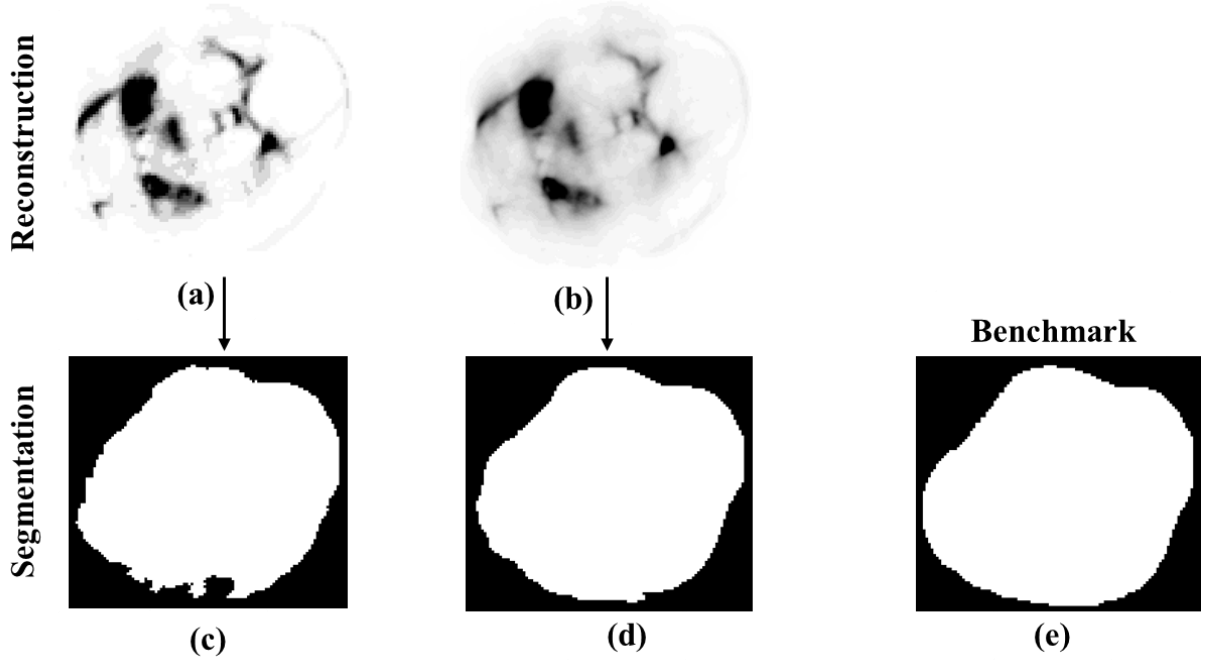

Figure 4.2. An example showing the effect of reconstruction parameters on segmentation performance. (a) and (b) The slices reconstructed from two different parameters. (c) and (d) The corresponding segmentation results. (e) The benchmark of segmentation for comparison.

4.3.1 Framework of parameter optimisation for iterative reconstruction

The framework of parameter optimisation for iterative reconstruction integrates the reconstruction and segmentation process as a whole as shown in Figure 4.3. In OPT a tomogram is referred to as $I_{(z,\beta,\theta)}$, with z and β representing the pixel position of tomogram at the projection angle θ. The 3D image is obtained by implementing the iterative reconstruction algorithm $f(\alpha)$ on the tomograms as $R^{\alpha}_{(x,y,z)} = f(\alpha)\, I_{(z,\beta,\theta)}$ with α being the parameters required for iterative reconstruction. The reconstructed results can further be segmented according to a specific criterion given the data, achieving the segmentation result $S^{\alpha}_{(x,y,z)}$ depicted in Figure 4.3, where $S^{\alpha}_{(x,y,z)} = g(R^{\alpha}_{(x,y,z)})R^{\alpha}_{(x,y,z)}$. Therefore, the segmentation result can be formulated as:

$$S^{\alpha}_{(x,y,z)} = f(\alpha) I_{(z,\beta,\theta)}\, g\left[f(\alpha)\, I_{(x_\theta,y_\theta,\theta)}\right] \tag{3}$$

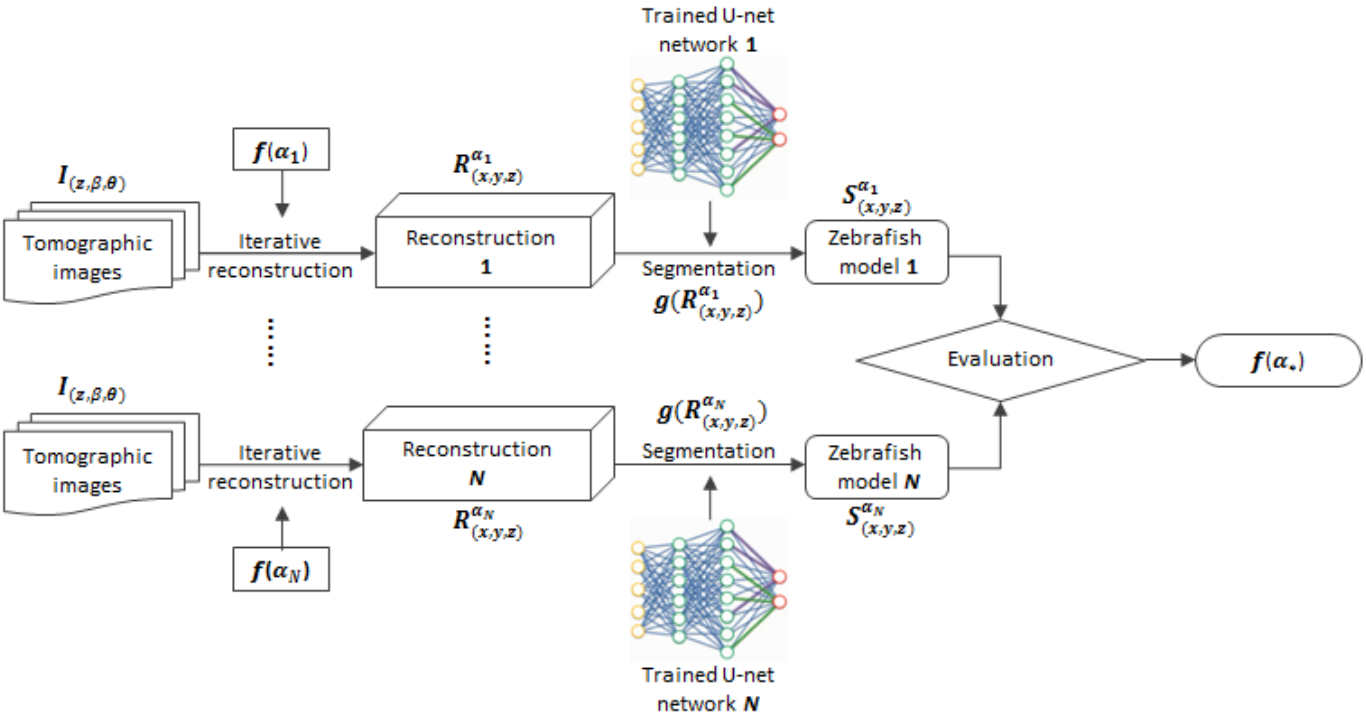

Figure 4.3. The framework for parameter optimisation for iterative reconstruction based on the corresponding segmentation performance. The 2D U-net [29] convolutional neural network is applied to train the segmentation model within each parameter group.

with g indicating the global function term for segmentation. Taking its high performance in biomedical image segmentation into account, we use the 2D U-net [29] convolutional neural network for our segmentation work. This means that, given the same tomogram, training the segmentation network with the 3D image reconstructed from different α will produce different network outputs for segmentation. However these differences originally result from the reconstruction parameter α rather than the network itself given the same configuration. From this notion the optimisation of α can be approximately transferred to

a search for a better α that produces 3D image for a better segmentation, with the idea that the benchmark of the segmentation is known; e.g. the zebrafish model in our work.

The diagram of the pipline for the optimisation is depicted in Figure 4.3. For the same tomogram set, it is assumed that there are *N* 3D image groups $\{R^{\alpha_1}_{(x,y,z)},\ldots, R^{\alpha_N}_{(x,y,z)}\}$ produced from iterative reconstruction functions $\{ f(\alpha_1),\ldots, f(\alpha_N)\}$ with $\{\alpha_1,\ldots, \alpha_N\}$ representing the variation of parameters. By evaluating the *N* 3D image groups based on their segmentation performances, we can achieve the best reconstruction parameter ranging from α_1 to α_N. If there are *K* samples for reconstruction and segmentation, then we have $R^{\alpha}_{(x,y,z)} = \{R^{\alpha}_{1(x,y,z)}, \ldots, R^{\alpha}_{k(x,y,z)}, \ldots, R^{\alpha}_{K(x,y,z)}$ and $S^{\alpha}_{(x,y,z)} = \{S^{\alpha}_{1(x,y,z)}, \ldots, S^{\alpha}_{k(x,y,z)}, \ldots, S^{\alpha}_{K(x,y,z)}\}$. It is worth mentioning that the segmentation network used in each 3D image group is internally trained rather than training it in a global scale across groups. This is because it is considered from an experimental perspective, more practical and valuable to train a segmentation network based on the data from the same reconstruction method, excluding the network preference when training it on the data across reconstruction approaches. With respect to segmentation network we employ the U-net CNN [29] because of its high performance in bio-medical image segmentation, generating a segmentation network group $\{ g(R^{\alpha_1}_{(x,y,z)}),\ldots, g(R^{\alpha_n}_{(x,y,z)}) \ldots, g(R^{\alpha_N}_{(x,y,z)} \}$. With the internal-trained segmenation network, evaluation will be performed to choose the group which has the highest performance, simultaneously finding the optimal iterative reconstrucion parameter $f(\alpha_*)$. There are several parameters required in the OSEM iterative reconstruction algorithm, but we focus on the two most customary ones, i.e. iteration number and initial reconstruction, as η and γ respectively. The different combinations of η and γ comprise $\{ \alpha_1 ,..., \alpha_n ,..., \alpha_N \}$, meaning that if $\eta = \{\eta_1, \ldots, \eta_i, \ldots, \eta_p\}$ and $\gamma = \{\gamma_1, \ldots, \gamma_j, \ldots, \gamma_q\}$, then $\alpha_n = (\eta_{i,} \gamma_j)$ and $N = p \times q$.

4.3.2 Segmentation approach

In order to provide a reliable and effective segmentation approach for reconstructed slices, CNN is employed as a result of its recent promising performance in medical image segmentation. As for our data, the zebrafish samples are transparent. It is challenging for traditional segmentation approaches to segment the foreground from the background when their intensities are very similar. A CNN can learn the structural and context information at different scales of resolution and, in that, it differs from traditional segmentation methods. For this reason, a CNN is very suitable for our research questions. We define our segmentation task as a binary segmentation on transparent samples in intensity image space. This means a small network such as 2D U-net rather than a complex network, is more desirable for our problem.

1) Network structure

The 2D U-net segmentation network [29] feeds 2D images as input layer, i.e. the reconstructed slices from the 3D image. Overall, the network contains encoder, decoder and a *Merge* layer between them as shown in Figure 4.4. In both the encoder and the decoder, there are 4 *Convolutional* layers and within each individual layer two 3x3 *Conv-*

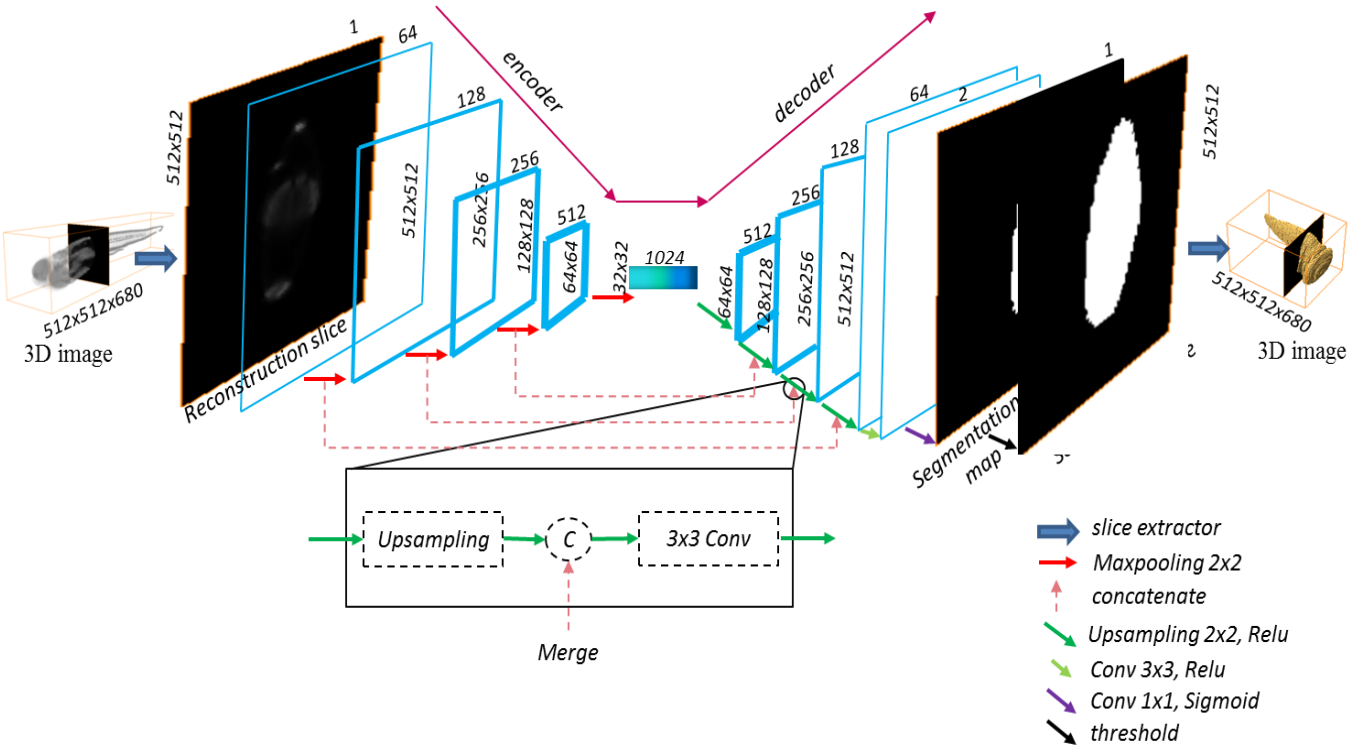

Figure 4.4. The structure of the 2D U-net network for zebrafish slices. Each slice is fed into the network as a single sample. The network contains both encoder (down layers) and decoder (up layers) for the deep CNN. The encoder is accomplished by a convolution and a max pooling operation while the decoder consists of a convolution and an upsampling operation. The *Maxpooling* and *Upsampling* layers are separately represented by red and green arrows. The *Convolution* layers are implemented with a 3x3 kernel at each depth of the encoder and decoder. Between similar layers on both sides there is a merge operation, allowing deep convolution layers to be merged with more shadow convolutional layers. *c* is the concatenation operation to merge layers from different depths.

olution layers and one *Dropout* layer are integrated. Different depths in the encoder and the decoder are separately connected by *Maxpooling* and *Upsampling* layers. The bridge-like *Merge* layer between the symmetric layers combines deep *convolution* layers and shadow ones. This typically improves the performance in segmentation problem. As the *Output* layer, the map activated by Sigmoid function [83], reflects the response to the zebrafish segmentation ranging from 0 to 1. The segmentation mask is generated when implementing a threshold on the map.

2) Network training

A. Training scheme

The segmentation network for zebrafish in each α_n -specified 3D image group is independently trained. The number of segmentation networks for the parameter optimisation framework is dependent on the parameter combination, as $N = p \times q$ for two parameters in our case. For a specific group $R^{\alpha_n}_{(x,y,z)}$, a certain ratio, typically small, of reconstructed slices from the 3D image are sampled at even intervals for training while the rest, a large ratio, are used for testing. The rationale for training on a small rather than large ratio of data is due to the fact of information redundancy among adjacent slices in 3D. Moreover, this can, to a large extent, reduce the workload of manual labelling. With a smaller ratio of data for training, the labelling for a single zebrafish could still be hundreds of slices. The image size of a typical OPT image is 512x512x1360. Here 1360 indicates the number of slices in the image of 512x512 per slice. To further decrease the labelling workload and make it more efficient, an interpolation approach is applied. The tool for interpolation labelling is available in software [63]. The results of interpolation labelling can be further verified manually and efficiently. The 3D images from the FBP reconstruction are used for labelling because of its capacity of offering comprehensive information.

Within each group the training slices and the corresponding labelled maps are used to train the segmentation network that is constructed referring to the work in [29]. Different from their network, the size of feature map after each convolutional layer maintains the same. The *Re*LU activation is used for all convolutional layers except for the last one which employs the sigmoid activation such that the output of the network ranges from 0 to 1. Another difference between the U-net network and ours is that we employ the simplest binary cross entropy as the loss function without considering the weight of each pixel in the image. The loss energy function would be:

$$E = \sum_{X \in \Omega} y(X)\log(\hat{y}(X)) + (1 - y(X))\log(1 - \hat{y}(X)) \quad (4)$$

where $y(X)$ is the labelled value at the pixel position $X \in \Omega$ with $\Omega \subset Z^2$, i.e. $y(X) \in \{0,1\}$. $\hat{y}(X)$ represents the predicted value at the same pixel position. The network is trained with the Adam optimizer [84] implementing Keras [85].

B. Learning rate

In the framework of stochastic gradient descent (SGD) [86],[87] optimisation technique for machine learning problem, the learning rate is considered to be carefully chosen to guarantee the convergence of the loss function. In order to set an effective learning rate to train the segmentation network, we first need to observe the intrinsic correlation between the data and the learning rate. Therefore, the different-fixed-learn-rate scheme is first applied to the data to investigate the different loss decay profiles. The profile of the loss function with an increasing epoch, using different fixed learning rates, is presented in

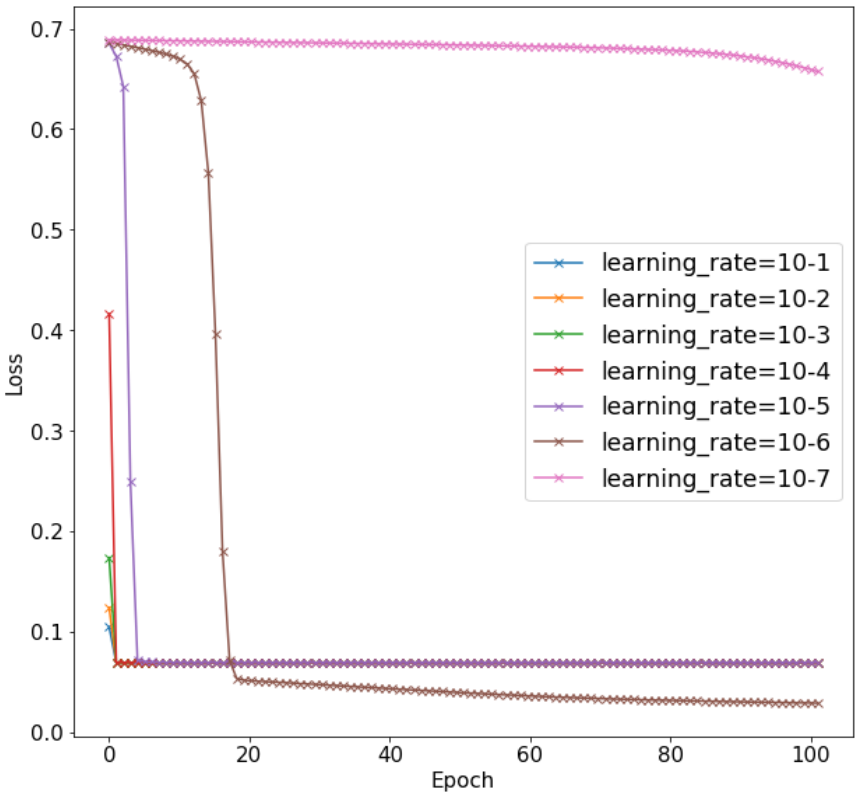

Figure 4.5. The profiles of the decay loss for different learning rates in 100 epochs. The learning rates observed are from 10^{-1} to 10^{-7}.

Figure 4.5. It easily and quickly falls into local minimum when the learning rate is set to or larger than 1e-5. To avoid this, the learning rate is supposed to be smaller than 1e-5. But when the learning rate is equal or smaller than 1e-7, the loss decreases extremely slow. 1e-6 is therefor considered to be a good initial learning rate for the data. However, as the epoch increases and the loss decreases, the loss decreases very slowly with the small learning rate 1e-6.

We observe a correlation between our data and learning rate. This can be seen in Figure 4.5, where loss curves for decreasing learning rate are plotted. As the learning rate increases, the learning process quickly drops to the local minimum. To avoid the learning process from falling into the local minimum, a small learning rate is required in the beginning of the training process while a relatively larger learning rate is lately needed to avoid the cost of extremely slow convergence. Moreover, the learning rate increase is supposed to be flat in the beginning to avoid the local minimum, while much steeper in the end to decrease the convergence cost. To meet these requirements, the learning rate scheme is designed as:

$$lr^{(i+1)_e} = lr^{i_e} * \lambda^{1+N_{i_e}} \quad (5)$$

where $lr^{(i+1)_e}$ and lr^{i_e} represent the learning rate at the ith and $(i+1)$th effective epoch respectively. An epoch is considered to be effective only when it decreases the loss function. For an effective epoch the learning rate will be recorded and used for the next update, while the learning rate of ineffective epoch will be propagated to the next epoch.

This means that if the current epoch fails to decrease the loss function, the same learning rate will be used for the next epochs until an effective epoch emerges. In Eq. (5) N_{i_e} counts the effective epochs and λ indicates the base of the exponential function which is much close to 1 but greater than 1, which is set as 1.001 for our experiments. We use the effective epoch count rather than epoch as the exponential power, to prevent the loss function from falling into the local minimum at the early stage and to limit the growth rate of learning rate at the late stage around the global optimal solution, resulting from a number of ineffective epochs. The initial learning rate is set as 1e-6 and we set the upper limit as 1e-4 to avoid divergence as the learning rate increases.

In Figure 4.6 we compare the loss decrease profiles between the fixed learning rate (1e-6) and the proposed learning rate in Eq. (5). It is observed that the proposed scheme starts from a point in the network which has a larger loss, but as the learning rate tardily increases the loss decreases slowly avoiding the local minimum. However, as the epoch increases, the loss rapidly falls down and reaches a smaller level that a fixed learning rate 10^{-6} fails to obtain.

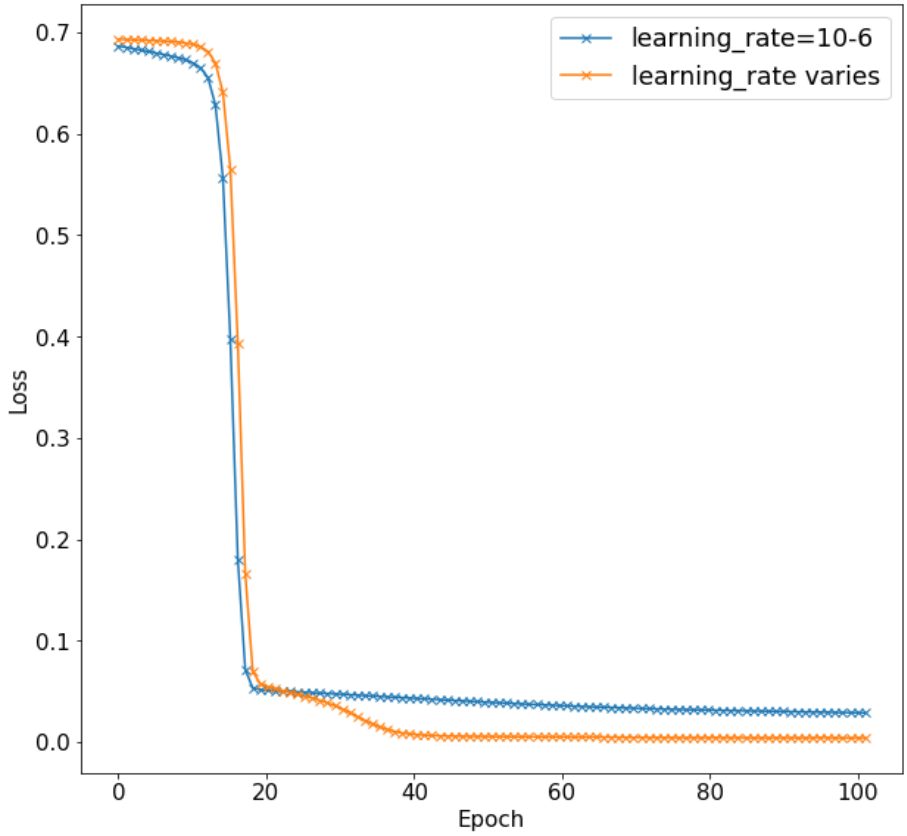

Figure 4.6. The comparison of the decay loss between learning rate 10^{-6} and the proposed learning rate scheme in 100 epochs. The proposed learning rate increases from 10^{-6} to 10^{-4}.

3) Segmentation

The segmentation describes the process of implementing the trained network on the *k*th test voxel $R^{\alpha_n}_{k(x,y,z)}$. We have a 2D kernel for training the segmentation network. It shows limited ability to consider the relationship between slices. It is assumed that the segmentation from network $g(R^{\alpha_n}_{(x,y,z)})$ is indicated as $M^{\alpha_n}_{(x,y,z)} \in \{0,1\}$, a binary map corresponding to the testing voxel. Considering the correlation between adjacent slice, a refining post-processing is introduced as follows. If $M^{\alpha_n}_{(x,y,z)} \oplus M^{\alpha_n}_{(x,y,z-1)} = 1$ and $M^{\alpha_n}_{(x,y,z)} \oplus M^{\alpha_n}_{(x,y,z+1)} = 1$, then $M^{\alpha_n}_{(x,y,z)}$ is set to equal to $M^{\alpha_n}_{(x,y,z-1)}$ and $M^{\alpha_n}_{(x,y,z+1)}$. This process particularly works for correcting the isolated segmentation error in *Z* direction. The segmentation result after the refined process refers as $S^{\alpha_n}_{(x,y,z)}$.

4.3.3 Evaluation criterion

The evaluation component as depicted in Figure 4.3 is accomplished by figuring out the group which has the best segmentation performance using the internally trained network, given the 3D zebrafish data and *N* different parameter groups $\{\alpha_1,\ldots,\alpha_N\}$. Different from 2D image segmentation, evaluation of image segmentation in 3D should be implemented based on a unit of 3D image because the slices are well ordered. This means that each 3D sample should be independently evaluated, rather than evaluating all the slices in 2D across samples. Because what interests us is not only the overall performance of segmentation on image slices but also the profile of performance change along the ordered slices, such as how the performance varies from the tail to head for zebrafish. Taking this into account the objective function for optimisation is formulated as follows:

$$\alpha^* = \min_{\alpha} \frac{1}{K} \sum_{k=1}^{K} \frac{\sigma_{-}(F1(S^{\boldsymbol{\alpha}}_{k(x,y,z)}))}{F1(S^{\boldsymbol{\alpha}}_{k(x,y,z)})} \tag{6}$$

K is the number of samples used for evaluation. For each sample, i.e. a zebrafish 3D image excluding the training slices in our experiment, both the overall performance in 3D and negative deviation σ_{-} of all slices to the overall performance are considered. The criterion in Eq. (6) for evaluation is defined as the modified coefficient of variation of F1-score (MCVF1). The negative deviation $\sigma_{-}(F1(S^{\boldsymbol{\alpha}}_{k(x,y,z)}))$ is defined as the standard deviation of F1 score [88] for the slices that perform worse than that of the overall 3D volume. $F1(S^{\boldsymbol{\alpha}}_{k(x,y,z)})$ gives the overall segmentation performance of the 3D volume for sample *k* with reconstruction parameter α. In our work this is accomplished by calculating the *F*1 scores for the whole segmentation volume $S^{\boldsymbol{\alpha}}_{k(x,y,z)}$. The aim of the parameter optimisation is to find the optimal α which produces 3D image group that has a maximum overall performance for segmentation as well as minimum negative deviation for performance. The details of experimental implement regarding to the segmentation evaluation of 3D image will be presented in the experimental section.

4.4 Experiments

In this section, we will first give an example to show the streak artefacts produced in the FBP reconstruction, for comparison followed by a result with artefacts eliminated, using iterative reconstruction method. The second part of the experiments is the parameter optimisation for iterative reconstruction, implemented on two zebrafish datasets cleared with different protocols. In the third experiment, we investigate the effects of different reconstruction methods, i.e. the FBP and iterative reconstruction, on segmentation performance, taking the streak artefacts into account.

4.4.1 Streak artefacts and elimination

In this section an intuitive comparison between the FBP [68] and iterative reconstruction [28] on a zebrafish for our OPT imaging system is given. There are quite dense but small-sized GFP [89] signals inside the zebrafish, which provides an extreme case regarding to how the streak artefacts are produced in OPT imaging and reconstruction. Figure 4.7 (a) and 4.8 (a) show the same tomogram which is one of the 400 ones evenly acquired in a full revolution. The corresponding reconstructed volumes are presented in Figure 4.7 (b) and 4.8 (b) from which a large difference can be observed. To further zoom in and visualize the difference we use both maximum projection along Z direction (Figure 4.7 (c) and 4.8 (c)) and 3D volume visualization (Figure 4.7 (d) and 4.8 (d)).

With the results in Figure 4.7 and 4.8, for both algorithms the pre-processing on the tomograms includes background subtraction and centre of rotation (CoR) correction in Chapter 2. The FBP reconstruction is implemented as elaborated in cf. § 2.3.2. For iterative reconstruction the iteration number η is set as 10 and the 3D image from the FBP is used as the initial reconstruction γ in this example. From the observation of different reconstructed results, we can see that the iterative reconstruction, in a superior manner, outperforms the FBP in terms of artefact suppression on the given data.

4.4.2 Parameter optimisation

To implement the experiments for the parameter optimisation, first the dataset and experimental settings are introduced. The iteration number and initial reconstruction are studied and optimized for reconstruction process. In this section, the details of experiments for optimizing these two parameters are explained.

1) Dataset and experimental settings

In order to implement the experiments for parameter optimisation, 6 zebrafishes are used for OPT imaging. They are split into two groups and are prepared with different protocols that result in different contrast and intensity distributions. Figure 4.9 shows two example images of zebrafish in bright-field mode of which each sample corresponds to a

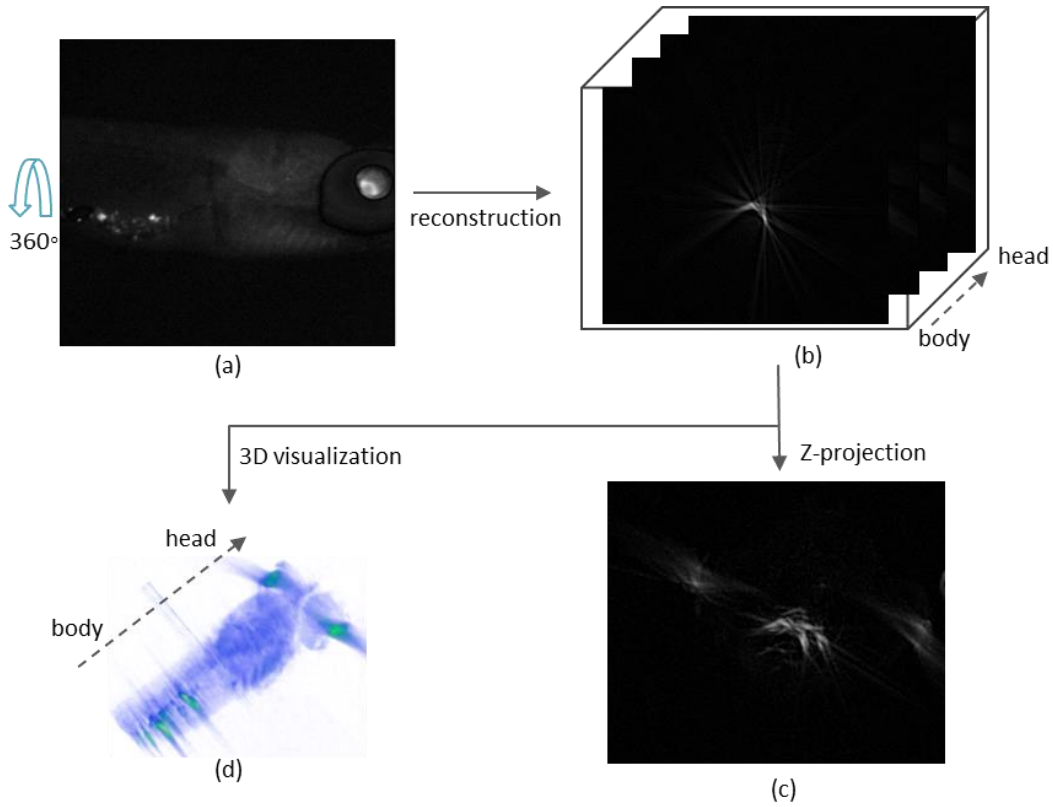

Figure 4.7. Streak artefacts existing in OPT reconstruction with the FBP reconstruction. (a) The tomogram of zebrafish in fluorescence mode. (b) Streak artefacts existing in the reconstructed slices using the FBP algorithm. (c) Z-projection of all reconstructed slices along with streak artefacts. (d) 3D volume rendering with streak artefacts.

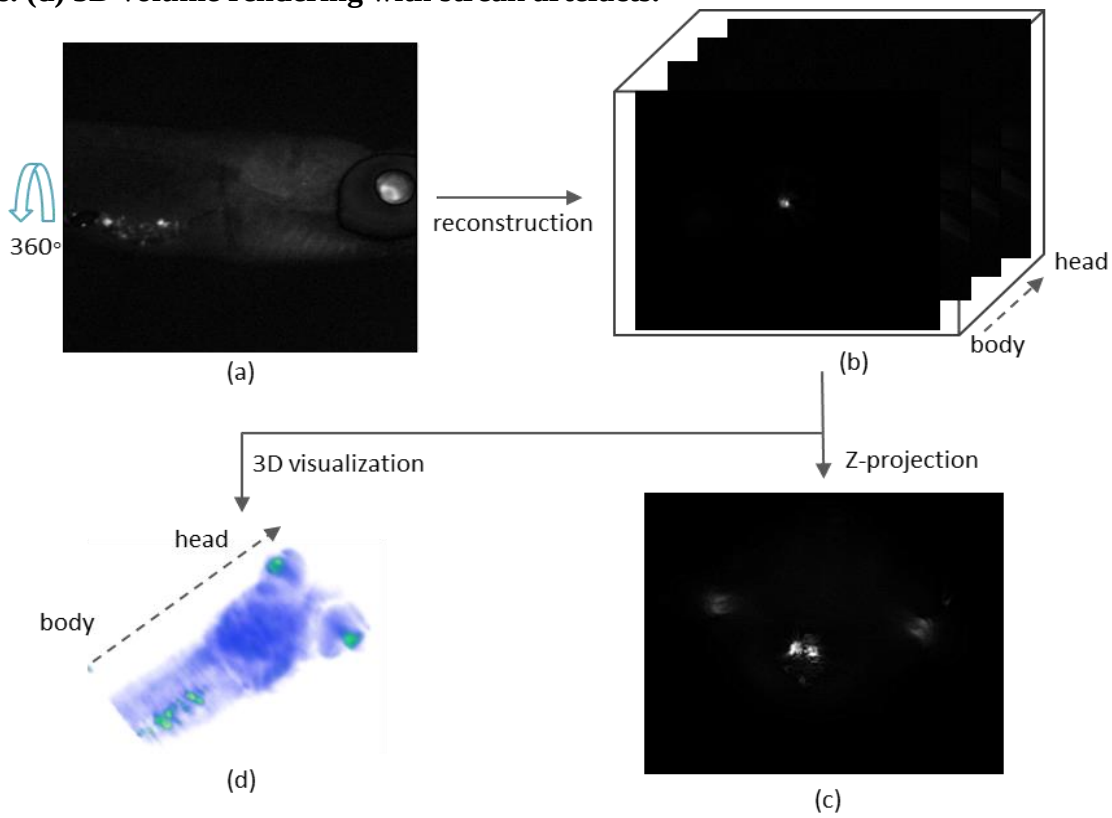

Figure 4.8. Streak artefacts eliminated with OSEM reconstruction in OPT. (a) The tomogram of

zebrafish in fluorescence mode. (b) Streak artefacts removed in the reconstructed slices using OSEM algorithm. (c) Z-projection of all reconstructed slices without streak artefacts. (d) 3D volume rendering with no streak artefacts.

different protocol for sample preparation. The motivation for using bright-field rather than fluorescence images is that, in our imaging system, bright-field images provide the outline information of a zebrafish. This can provide more prior knowledge to benchmark for segmentation. Figure 4.9 (a) corresponds to the tomogram of 5 *dpf* cleared zebrafish with BABB protocol [20], while (b) displays the 25 *dpf* zebrafish with CUBIC protocol [90],[91]. In the bright-field mode, we can easily observe the difference of intensity distribution between them. For each preparation protocol or dataset, there are three zebrafishes studied for parameter optimisation. Each reconstructed sample, i.e. zebrafish 3D image, consists of 1360 slices produced from a 400 tomogram image set using the reconstruction algorithm, compromising 4080 slices for each group or experimental implement.

We study the two most problematic parameters, i.e. iteration number η and initial reconstruction γ. First, for each dataset the effect of iteration number on segmentation performance is investigated. To this end, 5 groups of 3D images reconstructed from different iteration numbers are generated, combing the cost of computation and effectiveness of the reconstruction. Each group corresponds to one of five iteration numbers, i.e. $\eta = \{5, 10, 15, 20, 25\}$. We consider 5 to be a reasonable step size for the assessment of reconstruction performances based on different numbers of iteration, concerning the computational expense and experimental requirements.

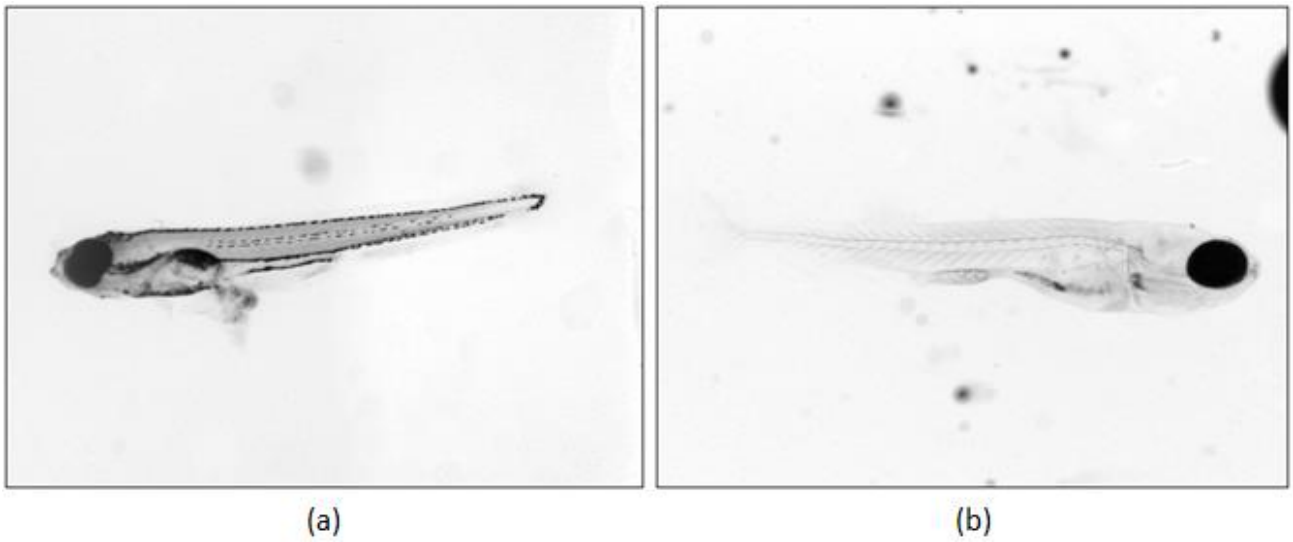

Figure 4.9. Samples of zebrafish with different preparation protocols in the bright-field mode. (a) One example of a tomogram for the 5 *dpf* zebrafish clearing with BABB [20] protocol. (b) One example of tomogram for the 25 *dpf* zebrafish cleared with CUBIC [90], [91] protocol.

The iteration number η is optimized by comparing the segmentation performance of each group. For initial reconstruction γ we compare the performance with an initial 3D

image from the FBP results (FBP-initial) and zeros (No-initial). To obtain the segmentation network all the zebrafish slices within each group are evenly distributed into training set (20%) and test set (80%). The segmentation network within each group is trained with the validation rate as 10%. The segmentation ground truths are labelled based on the FBP results. The segmentation performance MCVF1 of each group consists of overall F1 scores in 3D scale and the corresponding negative deviation on the test data as depicted in cf. § 4.3.2.

2) Iteration number and initial reconstruction

A. Experiments on 5 *dpf* zebrafish

The first data used in the experiments are three 5 *dpf* zebrafish are prepared with the BABB protocol [20]. The MCVF1 performance of each group defined in cf. § 4.3.2 and the performance of individual samples are presented in Table 4.1 and Table 4.2. The two tables show the performance differences of different initial reconstruction settings, with Table 4.1 presenting the results with the No-initial reconstruction setting while Table 4.2 corresponding to the FBP-initial results. Results are obtained based on the same training configuration of segmentation network.

For each sample with a particular iteration number, the performance consists of overall 3D F1 score $F1$ and negative deviation $\sigma_{-}(F1)$ of all slices. Such as for the Fish1 with 5-iterations, 98.23% represents $F1$ and 2.78% is $\sigma_{-}(F1)$. The smaller the MCVF1 is, i.e. higher $F1$ and smaller $\sigma_{-}(F1)$, the higher segmentation performance is. The results of the highest segmentation performance for each sample across iteration numbers are in bold. From the results obtained on the 3 zebrafishes, 10-iterations achieves the best overall performance for both No-initial and FBP-initial reconstruction. Regarding the different initial schemes, the FBP-initial method outperforms the No-initial approach in terms of three segmentation performances yielded with the same iteration number.

Table 4.1 and Table 4.2 present quantitative measures for segmentation performance on the 3D images. It, however, does not provide performance details of each slice inside of the 3D volume. In order to achieve these segmentation performances of all slices within each sample, each individual 3D image needs to be investigated. Figure 4.10 and 4.9 provides an example with that on the first zebrafish. Slices from the left to the right correspond to the zebrafish from the head to the tail. The F1_score of each slice ranges from 0 to 1. Each point in Figure 4.10 and 4.9 stands for a F1 score of one slice. The value of 1.0 on the left and right side of the figures implies a background slice in the reconstructed 3D data. Close to the background slices are the critical slices which are indistinguishable for segmentation. That is why they have quite low F1 score performances on both sides of the 3D data, i.e. the critical slices between the head or tail and background.

Table 4.1. Segmentation performance of iterative reconstruction implemented with various iteration numbers and No-initial reconstruction on the three 5 *dpf* zebrafishes.

No-initial	Fish1 (%)	Fish2 (%)	Fish3 (%)	MCVF1 (%)
5-iterations	98.23 (**-2.78**)	97.94 (-2.77)	97.88 (**-3.35**)	3.03
10-iterations	**98.24** (-2.82)	**98.14** (**-2.69**)	**97.94** (-3.37)	**3.02**
15-iterations	97.54 (-3.19)	97.38 (-3.63)	97.25 (-3.98)	3.70
20-iterations	97.34 (-3.10)	97.11 (-3.40)	96.91 (-3.84)	3.57
25-iterations	97.74 (-3.84)	97.70 (-3.10)	97.69 (-3.50)	3.56

Table 4.2. Segmentation performance of iterative reconstruction implemented with various iteration numbers and FBP-initial reconstruction on the three 5 *dpf* zebrafishes.

FBP-initial	Fish1 (%)	Fish2 (%)	Fish3 (%)	MCVF1 (%)
5-iterations	98.29 (-2.79)	98.01 (**-2.56**)	97.95 (-3.18)	3.55
10-iterations	**98.39** (**-2.63**)	**98.27** (-2.61)	**98.17** (**-3.16**)	**2.85**
15-iterations	98.29 (-2.82)	98.14 (-2.68)	98.06 (-3.18)	2.95
20-iterations	98.36 (-2.77)	98.04 (-2.77)	97.95 (-3.30)	3.00
25-iterations	98.31 (-2.76)	98.01 (-2.88)	98.02 (-3.57)	3.13

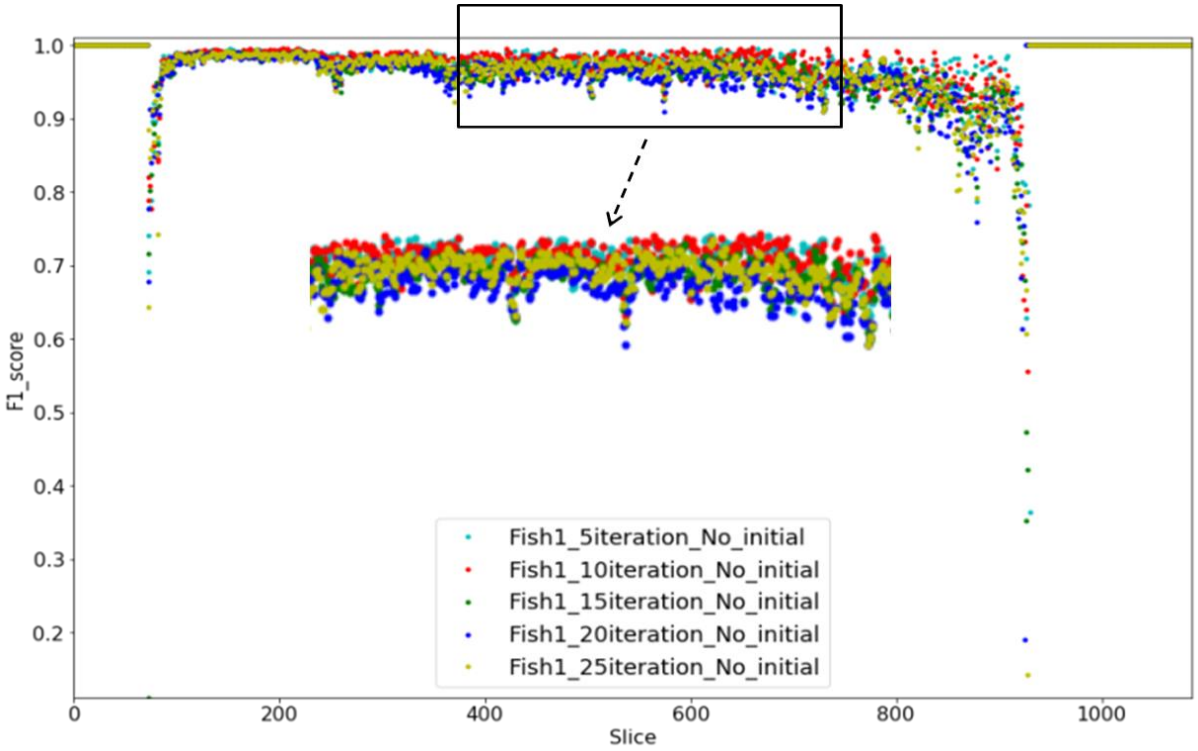

Figure 4.10. Segmentation performance of reconstructed slices with different iteration numbers in a No-initial setting on the 5 *dpf* Fish1. Each point represents the F1 score of each slice for segmentation. The rectangular area is zoomed.

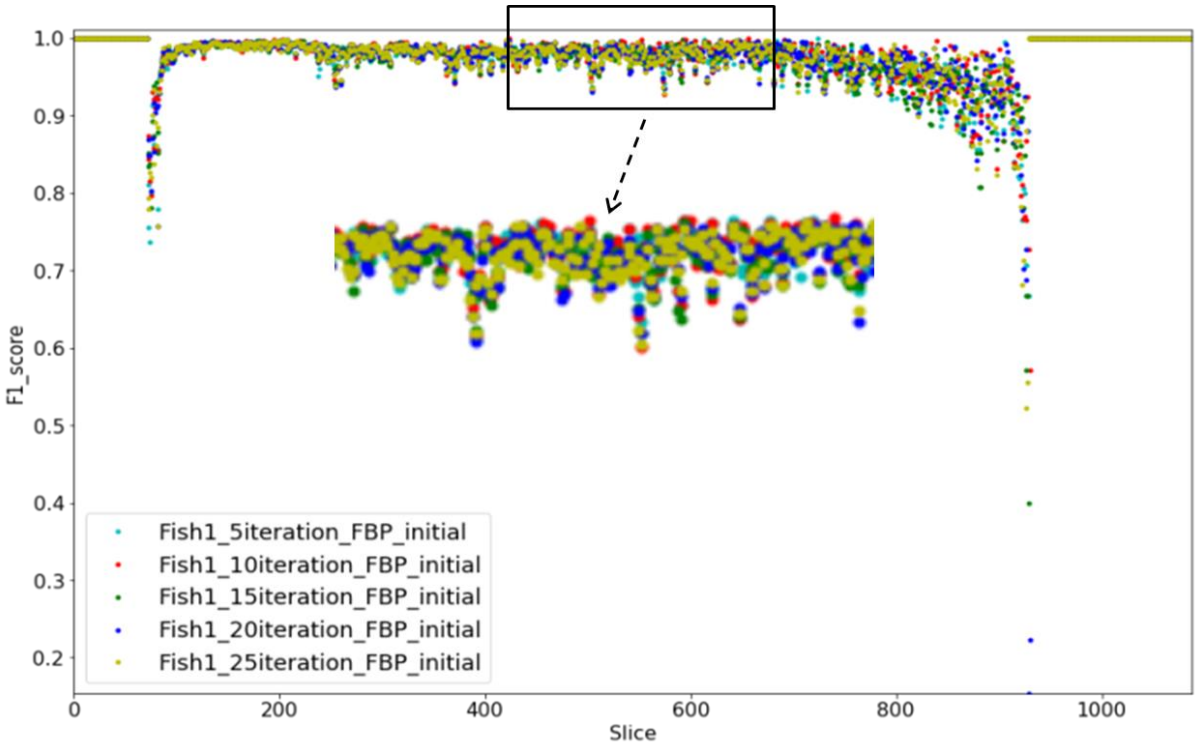

Figure 4.11. Segmentation performance of reconstructed slices with different iteration numbers in a FBP-initial setting on the 5 *dpf* Fish1. Each point represents the F1 score of each slice for segmentation. The rectangular area is zoomed.

By comparing the distribution of F1_score on all slices in Figure 4.10, we can also see that the 3D image group with 10-iterations has more points with larger F1_score and less with smaller F1_score, compared to other groups. This is in correspondence with the results of Fish1 in Table 4.1, i.e. larger $F1$ and smaller $\sigma\_(F1)$ value. Similar results can be observed in Figure 4.11 for FBP-initial reconstruction. The comparisons of segmentation performance on the 5 *dpf* zebrafishes reconstructed with different iterations, both for No-initial and FBP-initial, indicate that the reconstruction with the 10-iterations produces the most desirable results.

B. Experiments on 25 *dpf* zebrafish

As far as the variation of intensity distribution and experimental environment are concerned, three 25 *dpf* zebrafishes cleared with CUBIC protocol [90],[91] are also used for experiments. The performances of each sample and each 3D image group are demonstrated in Table 4.3 and 4.4, with MCVF1 corresponding to the performance of each group while $F1$ and smaller $\sigma\_(F1)$ showing the performance of each sample. As with Table 4.1 and 4.2, the best performance of individual sample and group is given in bold. Overall, the segmentation performance indicates that the FBP-initial reconstruction method outperforms the No-initial approach. Furthermore, in both cases, 10 iterations outperform other number of iterations, according to the MCVF1, $F1$ and $\sigma\_(F1)$ values. This is consistent with the observations regarding the 5 *dpf* zebrafishes.

However, compared to the 5 *dpf* zebrafishes, segmentation performances on the 25 *dpf* zebrafishes are generally lower and more deviated across 3D image groups. For example if we compare the Fish1 of both dataset in the No-initial case (in Table 4.1 and 4.3), the Fish1 of 5 *dpf* zebrafish as shown in Figure 4.9 (a), has a $F1$ range of [97.34, 98.24] that outperforms the range of [97.37, 97.97] for the Fish1 of 25 *dpf* zebrafish in Figure 4.9 (b). $\sigma\_(F1)$ of the 5 *dpf* Fish1 in Table 4.1 ranges from 2.78 to 3.84, smaller than that of 25 *dpf* Fish1 in Table 4.3 with the range from 3.51 to 4.83. Similar comparisons between the two datasets, corresponding to the two protocols, can be made for the other samples. In general, we conclude that the CUBIC clearing protocol makes the zebrafishes more transparent for OPT imaging compared to the BABB protocol. We need to acknowledge that a higher transparency of sample results in a higher similarity or a lower contrast between the foreground (zebrafish) and background tomograms and the 3D images, particularly at the object edge. Such 3D image will consequently have a lower segmentation performance and will be more sensitive to the number of iterations in the process of reconstruction.

Table 4.3. Segmentation performance of iterative reconstruction implemented with various iteration numbers and No-initial reconstruction on the three 25 *dpf* zebrafishes.

No-initial	Fish1 (%)	Fish2 (%)	Fish3 (%)	MCVF1 (%)
5-iterations	97.81 (-3.72)	96.51 (-9.24)	97.73 (-3.69)	5.72
10-iterations	**97.97** (**-3.51**)	**96.72** (**-5.78**)	97.84 (**-2.23**)	**3.95**
15-iterations	97.87 (-3.86)	95.18 (10.56)	**97.89** (-2.29)	5.79
20-iterations	97.86 (-4.40)	85.83 (-30.4)	97.82 (-3.32)	14.44
25-iterations	97.37 (-4.83)	76.08 (-40.2)	96.99 (-4.47)	20.79

Table 4.4. Segmentation performance of iterative reconstruction implemented with various iteration numbers and FBP-initial reconstruction on the three 25 *dpf* zebrafishes.

FBP-initial	Fish1 (%)	Fish2 (%)	Fish3 (%)	MCVF1 (%)
5-iterations	98.08 (-3.45)	**97.21** (-6.07)	98.17 (-3.08)	4.30
10-iterations	**98.29** (**-3.11**)	97.18 (**-5.75**)	**98.38** (**-2.58**)	**3.90**
15-iterations	97.71 (-3.99)	94.15 (-10.7)	97.48 (-3.76)	6.4
20-iterations	97.90 (-4.21)	91.56 (-25.4)	98.02 (-2.77)	11.60
25-iterations	97.90 (-3.73)	83.30 (-32.7)	97.84 (-3.28)	15.47

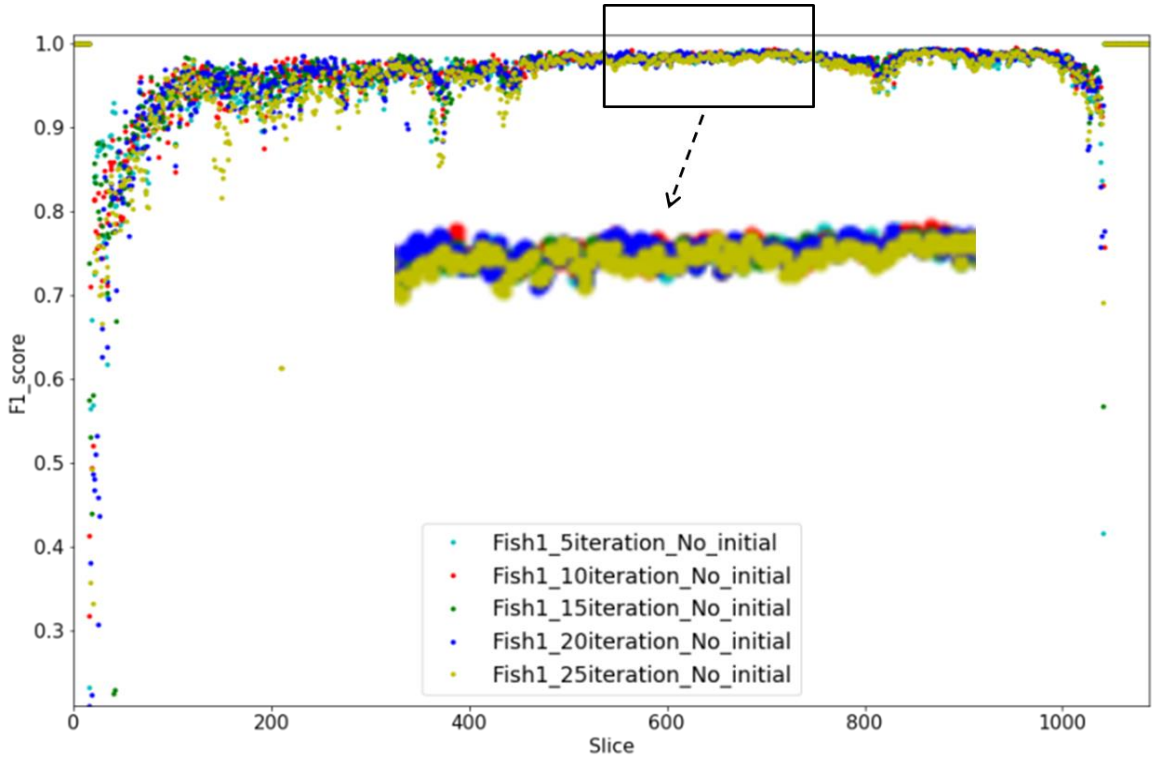

Figure 4.13. Segmentation performance of reconstructed slices with different iteration numbers in a No-initial setting on the 25 *dpf* Fish1. Performance is represented by F1 score of each slice. The rectangular area is zoomed.

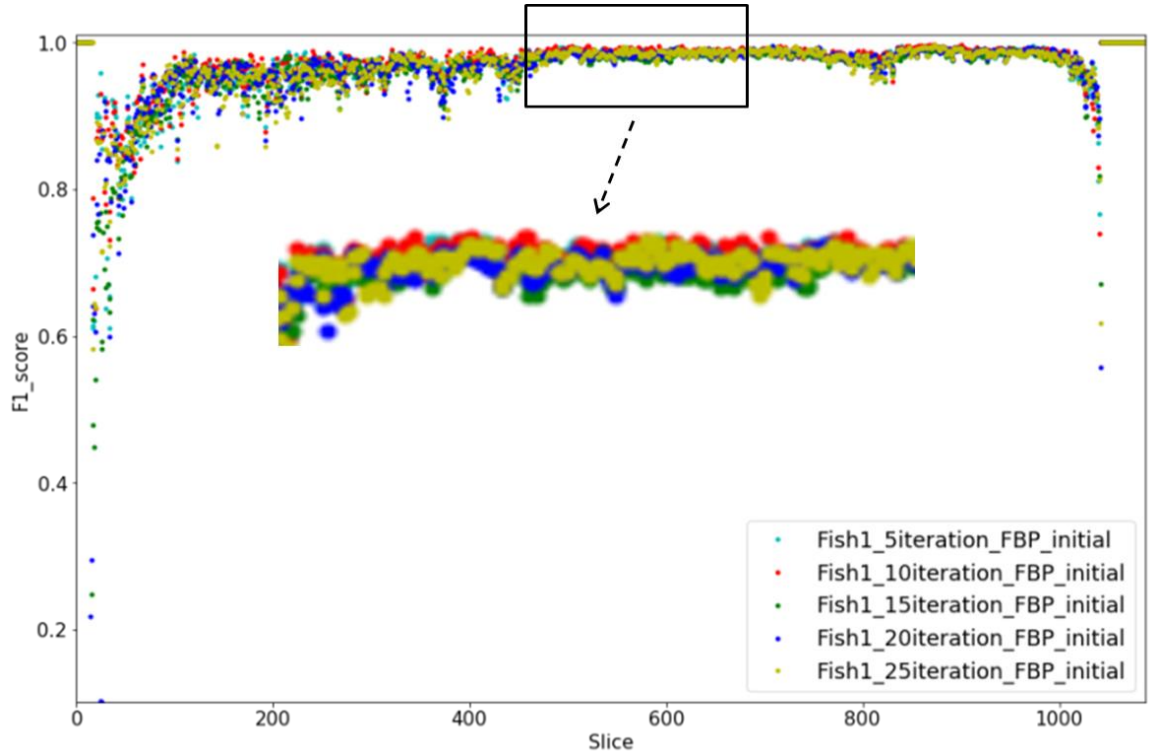

Figure 4.14. Segmentation performance of reconstructed slices with different iteration numbers in a FBP-initial setting on the 25 *dpf* Fish1. Performance is represented by F1 score of each slice. The rectangular area is zoomed.

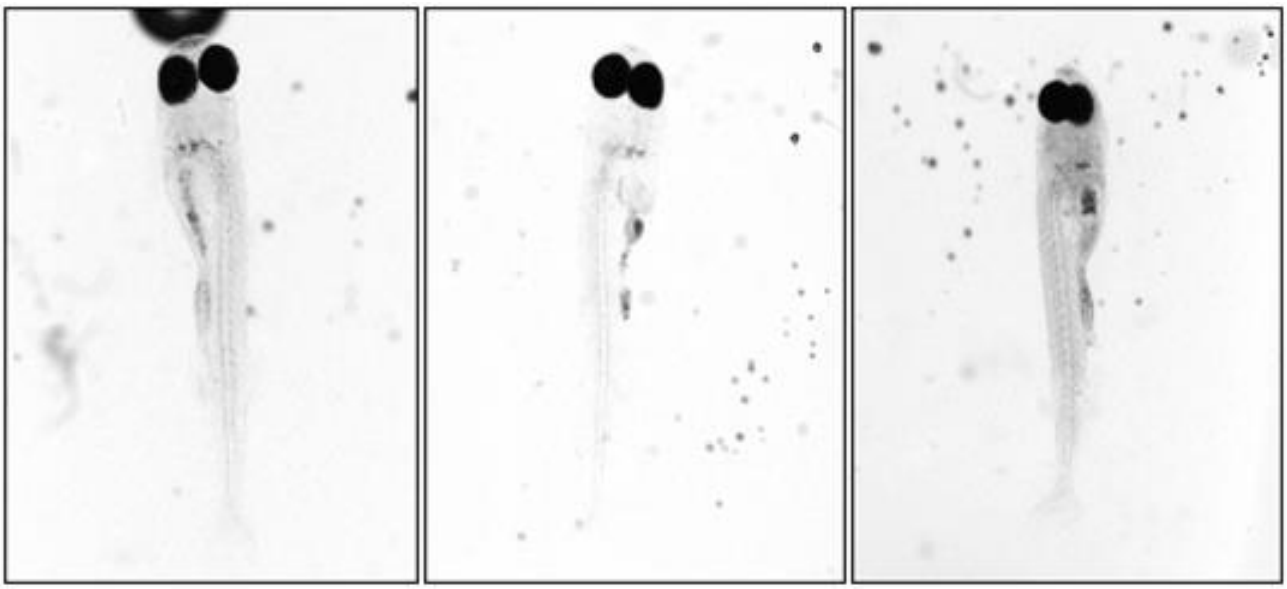

Figure 4.12. The tomogram of the 25 *dpf* Fish1, Fish2 and Fish3. They are shown in mounting orientation in the OPT imaging system. Fish2 has a lower contrast than the other two, with comparable background noise.

In Table 4.3 and 4.4 we can readily see that as iteration number increases the performance of sample Fish2 decreases dramatically whilst sample Fish1 and Fish3 decrease much less. This is because Fish2 has a lower contrast or a higher transparency as we can see from Figure 4.12. When the iteration number increases the information loss of the zebrafish body in the reconstruction is much more obvious. This makes it more difficult to be segmented correctly.

Regarding the performance of individual slices within the 25 *dpf* Fish1 for both No-initial and FBP-initial configuration, they are separately shown in Figure 4.13 and 4.14. For both cases, 10-iterations reconstruction outperforms other groups from either 2D slice or 3D volume scale.

4.4.3 Comparison of segmentation performance between OSEM and FBP

In this section the segmentation performance from the FBP reconstruction and the iterative reconstruction (OSEM) will be compared, experimented on the same datasets as for parameter optimisation, cf. § 4.4.2. In order to eliminate the contingency of gaining a good performance based a segmentation network that is trained on a fixed training set, different training sets are taken into account. They are evenly sampled from the 3D reconstruction slices with a different step size from 2 to 20, corresponding to the training ratio from 50% to 5%. 50% is considered to be a reasonably high training ratio for training a segmentation network in 3D OPT image, considering both accuracy and training cost. Higher training ratio might produce a bit higher accuracy, yet the training cost increases dramatically. As the aim of the comparisons among different reconstruction groups is to find the best-performed reconstruction parameters, rather than search for the global highest accuracy. Therefore, it is not necessary to train each network

with the highest training cost, e.g. a training ratio of 90%. The comparisons for both data are shown in Table 4.5 and 4.6. The performances are obtained with the same configuration for training segmentation networks.

In this experiment, the iteration number is set to 10 for the iterative reconstruction, because of its good performance, cf. § 4.4.2. In the training process of segmentation network, the number of epochs is set as 500 with batch size of 12 and each training process starts from a similar point in the network which can be seen from the loss and accuracy value. The MCVF1 of each 3D image group is calculated from individual samples, cf. § 4.3.2. The reconstruction method that has the smallest MCVF1 for each training ratio (bold) performs the best. By comparing the average MCVF1 we conclude that on both zebrafish datasets the FBP-initial iterative reconstruction achieves the best segmentation performance and are most desirable.

We further investigate the effect of streak artefacts on the segmentation performance. The average MCVF1 of different ratios of training set, produced with a specific reconstruction method, is seen as the criterion for assessing the overall performance of the reconstruction method. For the 5 *dpf* zebrafishes, the overall performances of the three reconstruction methods are 6.00, 3.90, and 3.83. Because the 5 *dpf* zebrafishes are cleared with the BABB protocol that maintains high specimen contrast; the pigments on the zebrafish skin are more concentrated, cf. Figure 4.9 (a). This introduces more streak artefacts in the FBP reconstructed slices. This explains the reason why iterative reconstruction methods (both No-initial and FBP-initial) highly outperform FBP method in Table 4.5. Different from the BABB protocol, the 25 *dpf* zebrafishes are cleared with CUBIC protocol. In this case, we obtain tomograms with lower contrast and the pigments are also less concentrated, introducing less streak artefacts in the FBP reconstruction. This allows the FBP reconstruction to produce 3D images achieving comparable overall performance (5.51) for segmentation, comparing to the iterative reconstructions (5.81 and 5.32).

Excluding the effect of streak artefacts on segmentation, we only look at the overall performance of OSEM reconstruction on the two different datasets in Table 4.5 and 4.6. The 5 *dpf* less transparent zebrafishes outperform the 25 *dpf* zebrafishes which are more transparent. When we compare the performances between the OSEM and FBP, it can be seen that the results for the 25 *dpf* zebrafishes are comparable, but the OSEM achieves better performance than the FBP for the 5 *dpf* zebrafishes. The reason for the difference is that the FBP reconstructions for the 5 *dpf* zebrafishes have much more streak artefacts than the 25 *dpf* zebrafishes do, which deteriorates the segmentation performance.

Table 4.5. Comparisons of segmentation performance using different reconstruction algorithms on the three 5dpf zebrafishes.

5*dpf*	**FBP**				**No-initial OSEM**				**FBP-initial OSEM**			
Training Ratio	**Fish1 (%)**	**Fish2 (%)**	**Fish3 (%)**	**MCVF1 (%)**	**Fish1 (%)**	**Fish2 (%)**	**Fish3 (%)**	**MCVF1 (%)**	**Fish1 (%)**	**Fish2 (%)**	**Fish3 (%)**	**MCVF1 (%)**
2 (50.0%)	98.02 (-2.57)	97.83 (-3.23)	98.01 (-3.76)	3.26	98.90 (-2.30)	98.92 (-2.18)	98.90 (-2.81)	2.46	98.87 (-2.17)	98.92 (-2.02)	98.86 (-2.67)	**2.32**
5 (20.0%)	97.10 (-3.17)	96.15 (-4.57)	96.61 (-5.53)	4.57	98.24 (-2.82)	98.14 (-2.69)	97.94 (-3.37)	3.02	98.39 (-2.63)	98.27 (-2.61)	98.17 (-3.16)	**2.85**
8 (12.5%)	97.02 (-3.29)	96.61 (-4.67)	97.02 (-5.50)	5.05	97.81 (-3.21)	97.89 (-3.17)	97.89 (-3.62)	3.40	97.65 (-3.17)	97.66 (-3.25)	97.63 (-3.21)	**3.29**
10 (10.0%)	94.86 (-5.54)	93.80 (-5.66)	95.08 (-7.40)	6.42	97.39 (-3.39)	97.28 (-3.64)	97.14 (-3.89)	3.74	97.50 (-3.29)	97.50 (-3.25)	97.16 (-4.19)	**3.68**
12 (8.30%)	94.99 (-5.77)	93.51 (-6.14)	95.04 (-6.32)	6.43	96.81 (-3.78)	96.53 (-4.15)	96.23 (-4.38)	4.25	97.22 (-3.26)	97.32 (-4.24)	97.04 (-4.58)	**4.15**
15 (6.70%)	95.26 (-5.29)	94.86 (-6.56)	95.76 (-7.32)	6.71	97.20 (-3.69)	97.04 (-3.89)	96.90 (-4.46)	**4.13**	97.22 (-4.26)	97.14 (-3.34)	97.05 (-4.87)	4.27
18 (5.60%)	94.28 (-5.91)	92.06 (-7.23)	93.60 (-7.06)	7.21	96.78 (-4.34)	96.80 (-4.36)	96.71 (-5.19)	4.79	96.80 (-4.60)	96.83 (-4.13)	96.67 (-4.54)	**4.57**
20 (5.00%)	93.61 (-6.89)	91.2 (-7.47)	93.31 (-8.90)	8.36	96.58 (-4.54)	96.23 (-5.63)	96.11 (-5.25)	**5.34**	96.30 (-4.80)	96.05 (-5.18)	95.65 (-5.90)	5.51
Average				6.00				3.90				**3.83**

Table 4.6. Comparisons of segmentation performance using different reconstruction algorithms on the three 25dpf zebrafishes.

5*dpf*	**FBP**				**No-initial OSEM**				**FBP-initial OSEM**			
Training Ratio	**Fish1 (%)**	**Fish2 (%)**	**Fish3 (%)**	**MCVF1 (%)**	**Fish1 (%)**	**Fish2 (%)**	**Fish3 (%)**	**MCVF1 (%)**	**Fish1 (%)**	**Fish2 (%)**	**Fish3 (%)**	**MCVF1 (%)**
2 (50.0%)	98.04 (-4.34)	98.11 (-3.51)	98.44 (-1.98)	3.34	98.85 (-2.42)	98.45 (-3.48)	98.91 (-1.95)	**2.65**	98.85 (-2.66)	98.47 (-3.76)	98.96 (-1.86)	2.79
5 (20.0%)	96.93 (-5.51)	96.70 (-5.41)	98.07 (-3.03)	4.78	97.97 (-3.51)	96.72 (-5.78)	97.84 (-2.23)	3.94	98.29 (-3.11)	97.18 (-5.75)	98.96 (-1.86)	**3.89**
8 (12.5%)	97.25 (-5.23)	96.67 (-5.65)	97.69 (-3.06)	4.78	97.95 (-3.85)	96.06 (-7.92)	98.15 (-3.07)	**5.08**	97.89 (-4.02)	95.76 (-7.77)	98.12 (-3.31)	5.17
10 (10.0%)	96.62 (-5.71)	96.55 (-5.42)	97.83 (-3.03)	4.87	97.67 (-3.99)	94.90 (-8.94)	97.91 (-3.02)	5.49	97.70 (-3.73)	95.73 (-7.18)	97.87 (-3.11)	**4.81**
12 (8.30%)	95.73 (-9.91)	95.78 (-6.40)	97.53 (-2.93)	6.65	97.49 (-4.18)	94.49 (-9.52)	97.74 (-3.63)	**5.99**	97.52 (-4.38)	94.58 (-10.5)	97.75 (-2.73)	6.07
15 (6.70%)	95.59 (-7.27)	95.96 (-5.21)	97.18 (-3.53)	**5.55**	97.14 (-4.82)	93.97 (-11.2)	97.33 (-3.74)	6.86	97.19 (-4.55)	94.47 (-8.38)	97.40 (-4.27)	**5.95**
18 (5.60%)	94.13 (-10.3)	95.70 (-5.82)	96.73 (-4.06)	7.05	97.07 (-5.35)	91.84 (-13.1)	97.12 (-4.17)	7.91	97.18 (-4.70)	93.54 (-11.7)	97.38 (-3.34)	**6.85**
20 (5.00%)	95.62 (-7.08)	94.30 (-9.99)	97.24 (-3.28)	7.08	96.81 (-6.07)	91.82 (-14.8)	96.96 (-3.45)	8.52	96.76 (-5.43)	92.08 (-10.7)	97.07 (-4.01)	**7.04**
Average				5.51				5.81				**5.32**

4.4.4 Discussion

In this section an overall experimental discussion will be given. In § 4.4.1 the qualitative comparison between the FBP and iterative (OSEM) reconstruction is presented, in terms of the elimination of artefacts in one specific zebrafish. This inspired and motivated us to go one step further and study the parameter optimisation for the iterative reconstruction with respect to its potential performance in OPT reconstruction. This means that the effect of different reconstruction parameters needs to be investigated. We accomplished this in § 4.4.2 by studying the two most problematic parameters, i.e. the number of iterations and the initial reconstruction, on two zebrafish datasets with different image intensity distributions. According to these experiments, the combination of 10-iterations and FBP-initial is proved to produce the most desirable and preferable 3D image, compared to the other combinations. Additionally, 10-iterations are also acceptable for reconstruction implementation concerning the computation cost. When comparing the segmentation performances across datasets, we find that the contrast rich dataset performs better, which is reasonable from theoretical perspective. Because a highly transparent sample produces a more indistinguishable intensity distribution in both tomogram and 3D image in OPT, therefore bringing more complications for the segmentation.

Followed by parameter optimisation, comparisons of segmentation performance between the FBP and iterative reconstruction are displayed in a quantitative manner. It is known that sample preparation plays a crucial role in the OPT imaging, as well as the 3D reconstruction process. One should realize that the BABB protocol provides higher specimen contrast that generally leads to a better 3D image from the iterative reconstruction and consequently achieves a higher segmentation performance, however introduces streak artefacts when using the FBP reconstruction. Moreover, with the BABB clearing protocol, the iterative reconstruction can eliminate the streak artefacts during the reconstruction process, so the segmentation result outperforms that of the 3D images from the FBP algorithm. With the CUBIC clearing protocol, both reconstruction methods are able to avoid the streak artefacts in the 3D image, therefore obtaining a comparable segmentation performance between different approaches. In this work the experiments are implemented on finite zebrafish samples. With the trend of high-throughput analysis on zebrafish, in the near future more samples will be considered to confirm this tendency.

4.5 Conclusions

The research presented in this chapter is the development and implementation of an iterative reconstruction, specifically OSEM, and the further exploration of approaches to optimize the reconstruction parameters. The OSEM algorithm produces superior 3D image in comparison with FBP algorithm in terms of streak artefact elimination when the signals in the tomograms are very concentrated. The method used for further improvement of the reconstruction is realized by optimizing the parameters for the OSEM algorithm,

which requires the evaluation of reconstructed 3D image. Restricted by the lack of benchmarks for reconstruction in real-life imaging, we have used an alternative approach that is inspired by the segmentation evaluation. Notably, the way of integrating segmentation evaluation into parameter optimisation for iterative reconstruction, may not result in the achievement of the globally optimal parameters. But to our best knowledge, it provides a good and reasonable way for guaranteeing an optimized and efficient reconstruction result, considering both the reconstruction quality and computational cost. It is worth point out that, even though the OSEM produces promising results for highly transparent samples, e.g. the 25 *dpf* Fish2 with 10 iterations, it could also be possible that a sample is too transparent to produce any significant reconstruction results with the same OSEM parameters. In such an extreme case, decreasing the iteration number might help recover more information in compromise with image blur.

4.6 Acknowledgement

The work is partially funded by China Scholarship Council (CSC). We would like to express our gratitude to Rob van Wijk (LACDR & IBL, Leiden, Netherlands) and Shuning He (Dana-Farber Cancer Institute, Boston, USA) for making available the fixated 5 *dpf* and 25 *dpf* fishes. We also would like to express our thanks to Hermes Spaink (LIACS, Leiden, Netherlands for his contribution to sample preparation and imaging.